THE JOURNAL OF BIOLOGICAL CHEMISTRY VOL. 283, NO. 51, pp. 35834–35844, December 19, 2008
Printed in the U.S.A.

Requirements for Protein Phosphorylation and the Kinase Activity of Polo-like Kinase 1 (Plk1) for the Kinetochore Function of Mitotic Arrest Deficiency Protein 1 (Mad1)*[S]

Received for publication, June 30, 2008, and in revised form, October 14, 2008 Published, JBC Papers in Press, October 15, 2008, DOI 10.1074/jbc.M804967200

Ya-Hui Chi[‡], Kerstin Haller[‡], Michael D. Ward[§], O. John Semmes[§], Yan Li[‡], and Kuan-Teh Jeang[‡1]

From the [‡]Molecular Virology Section, Laboratory of Molecular Microbiology, NIAID, National Institutes of Health, Bethesda, Maryland 20892 and the [§]Department of Microbiology and Molecular Cell Biology, Center for Biomedical Proteomics, Eastern Virginia Medical School, Norfolk, Virginia 23501

Mitotic arrest deficiency protein 1 (Mad1) is associated with microtubule-unattached kinetochores in mitotic cells and is a component of the spindle assembly checkpoint (SAC). Here, we have studied the phosphorylation of Mad1 and mapped using liquid chromatography-tandem mass spectrometry several phosphorylated amino acids in this protein. One phosphorylated residue, Thr[680], was characterized to be important for the kinetochore localization of Mad1 and its SAC function. We also found that in mitotic cells Mad1 co-immunoprecipitated with Plk1. Depletion of cellular Plk1 using small interfering RNAs and inhibition of the kinase activity of Plk1 using a kinase-dead mutant or a small molecule inhibitor attenuated Mad1 phosphorylation and its association with kinetochores. Collectively, these findings indicate mechanistic roles contributed by protein phosphorylation and Plk1 to the SAC activity of Mad1.

Faithful chromosome partitioning from a mother cell to her daughter cells is essential for maintaining euploidy. Loss of fidelity in chromosomal segregation creates aneuploidy that can contribute to oncogenesis (1–4). The mitotic spindle assembly checkpoint (SAC)[2] monitors the attachment of kinetochores to bipolar spindle poles and regulates proper chromosome segregation in mitosis (5). Mad1 is a component of the SAC (6) and is found as a heterodimer (7) with Mad2 at the nuclear pore complex as a cell enters mitosis (8). Later when the nuclear envelope commences breakdown, the Mad1·Mad2 complex moves from the nuclear periphery to spindle-unattached kinetochores (9–12). Current evidence suggests that Mad1 is required for Mad2 localization to kinetochores (12–14), and the association of Mad2 with the kinetochore is a prerequisite for its SAC function.

Recent studies indicate that Mad2 adopts two conformations (O-, open, and C-, closed) during the G_2 to M phases. At spindle unattached kinetochores, Mad1 binds a C-Mad2 (15–17). Kinetochore-bound Mad1-C-Mad2 recruits cytosolic O-Mad2 changing the latter to a form capable of Cdc20 binding (15, 16) and inhibiting the anaphase promoting complex/cyclosome (APC/C), an E3 ubiquitin ligase complex (18–20). Currently, the event(s) that regulates Mad1 movement from the nuclear pore complex to microtubule-unattached kinetochores is unknown.

Understanding how Mad1 activity is modulated is important for several reasons. First, aberrant Mad1 expression is linked to the development of human small cell lung cancer (21) and gastric carcinoma (22). Second, in genetically engineered *Mad1*$^{+/-}$ mice, reduced Mad1 function elevates the incidence of cancers (4), correlating SAC inefficiency with oncogenic proclivity in rodents (23–25). Third, several human cancer viruses target the SAC of the cells (26–29) in their transforming mechanism(s); and, Mad1 was identified as a cellular target for the human T-cell leukemia virus type 1 Tax oncoprotein (30, 31). Tax inactivation of the SAC function of Mad1 appears to contribute to human T-cell leukemia virus type 1 engendered adult T-cell leukemia (32).

Previously, human Mad1 was suggested to be phosphorylated in mitosis (30). However, the consequences of Mad1 phosphorylation have not been characterized. Here, we demonstrate that Mad1 is hyperphosphorylated when Plk1 is overexpressed and that the kinase activity of Plk1 is required for Mad1 to locate to microtubule-unattached kinetochores. We identified several intracellular phosphorylation sites in Mad1 and showed that loss of a Thr[680]-phosphorylated site in Mad1 converted the protein to a dominant negative mutant.

EXPERIMENTAL PROCEDURES

Plasmids, Antibodies, and Reagents—The Plk1 kinase-dead mutant K82M (33) was generated using the QuikChange II XL Site-directed Mutagenesis Kit (Stratagene, La Jolla, CA) according to the manufacturer's protocol. The primers used are 5′-gaggtgttcgcgggcatgattgtgcctaagtc-3′ and 5′-gacttaggcacaatcatgcccgcgaacacctc-3′. Rabbit Mad1 antibodies were raised against recombinant GST-Mad1-N (amino acids 1–301) or GST-Mad1-C (amino acids 402–718). The rabbit Mad1 anti-

* This work was authored, in whole or in part, by National Institutes of Health staff. The costs of publication of this article were defrayed in part by the payment of page charges. This article must therefore be hereby marked "*advertisement*" in accordance with 18 U.S.C. Section 1734 solely to indicate this fact.

[S] The on-line version of this article (available at http://www.jbc.org) contains supplemental Figs. S1–S4.

[1] Supported through intramural funding from the NIAID, National Institutes of Health. To whom correspondence should be addressed: Bldg. 4, Rm. 306, 9000 Rockville Pike, Bethesda, MD 20892-0460. Tel.: 301-496-6680; Fax: 301-480-3686; E-mail: kj7e@nih.gov.

[2] The abbreviations used are: SAC, spindle assembly checkpoint; Mad1, mitotic arrest deficiency protein 1; Plk, polo-like kinase; APC/C, anaphase promoting complex/cyclosome; HA, hemagglutinin; siRNA, small interfering RNA; PBS, phosphate-buffered saline; WT, wild type; DAPI, 4′,6-diamidino-2-phenylindole; CHAPS, 3-[(3-cholamidopropyl)dimethylammonio]-1-propanesulfonic acid; MS, mass spectrometry.

sera were first captured with protein A-agarose (Bio-Rad), and then affinity purified using GST-Mad1-N or GST-Mad1-C fusion proteins conjugated to Affi-Gel 10 (Bio-Rad). Commercial reagents were obtained as follows: monoclonal anti-Plk1 antibodies were from Invitrogen and Santa Cruz Biotechnology (Santa Cruz, CA); the human CREST antiserum was from Cortex Biochem (San Leandro, CA); the rabbit anti-Mad2 antibody was from Covance (Denver, PA); the rabbit anti-securin (PTTG) antibody was from Invitrogen; the rabbit anti-Aurora B and mouse anti-cyclin B1 antibodies were from Santa Cruz Biotechnology; anti-HA and anti-FLAG antibodies were from Sigma; monoclonal anti-BubR1 antibody was from MBL (Woburn, MA); monoclonal anti-Mps1 antibody was from Millipore (Billerica, MA); monoclonal anti-phospho-Ser/Thr/Tyr antibody (αpSYT) was from Abcam (Cambridge, MA). Validated synthetic siRNA duplexes targeting Plk1 (Hs_Plk1_7: 5′-CGCGGGCAAGAUUGUGCCUAA-3′) and Mad1 (5′-CAGCGATTGTGAAGAACATGA-3′ and 5′-CAGGACCA-AAGTGCTGCACAT-3′) were from Qiagen (Valencia, CA). Nocodazole, thymidine, and Plk1 inhibitor GW843682X were purchased from Sigma. Purified bioactive Plk1 protein was purchased from Cell Signaling Technology (Boston, MA).

Cell Culture and Transfection—HeLa cells were maintained in Dulbecco's modified Eagle's medium containing 10% fetal bovine serum and supplemented with 2 mM L-glutamine and antibiotics. Generation of stable cell lines expressing FLAG-tagged human Mad1 (HeLa-FlagMad1) was initiated by transfecting pCDNA-FlagMad1 plasmid into HeLa cells using Lipofectamine (Invitrogen). 24 h after transfection, cells were divided into 15-cm culture dishes and selected in complete medium containing 0.7 mg/ml G418. G418-resistant colonies were individually cloned and checked by Western blotting and PCR. Stable cell clones were maintained in medium supplemented with 0.3 mg/ml G418. Transfection of siRNA duplexes was performed using TransMessenger transfection reagent (Qiagen) according to the manufacturer's protocol.

Cell Synchronization—For synchronization, cells were treated with 2.5 mM thymidine for 12 h and released from the G_1/S block into fresh medium. 12 h after release, cells were treated with 2.5 mM thymidine again for another 12 h to obtain G_1/S-synchronized cells. G_2 phase cells were prepared by releasing G_1/S cells from double thymidine block for 7 h. M phase cells were prepared by a 5-h treatment with spindle toxin (*i.e.* 200 nM nocodazole) 7 h after cells were released from double-thymidine block.

Co-immunoprecipitation and Western Blotting—For co-immunoprecipitation, cells were washed twice with phosphate-buffered saline (PBS), harvested, and lysed with RIPA buffer (50 mM HEPES, pH 7.3, 150 mM NaCl, 2 mM EDTA, 20 mM β-glycerophosphate, 0.1 mM Na_3VO_4, 1 mM NaF, 0.5 mM dithiothreitol and protease inhibitor mixture (Roche Applied Science)) containing 0.5% Nonidet P-40 and then sheared using a 22-gauge needle. Cleared lysates were incubated with antibody-conjugated agarose beads for 16 h at 4 °C. The agarose beads were then washed 5 times with RIPA buffer. The co-immunoprecipitated proteins were analyzed by SDS-PAGE/Western blotting. For Western analyses, samples were transferred to polyvinylidene fluoride membranes, which were blocked with 0.2% I-Block (Tropix, Bedford, MA) in PBS and 0.1% Tween 20. The primary antibodies were used at 1:1,000 to 1:10,000 dilutions. For immunoblotting using αpSYT, membranes were blocked with 5% (w/v) bovine serum albumin in Tris-buffered saline containing 0.1% Tween 20 (TBST). The αpSYT antibody was diluted 1:2,000 in TBST. For secondary antibodies, alkaline phosphatase-conjugated anti-mouse or anti-rabbit (Sigma) was used, and detection was by chemiluminescence following the manufacturer's protocol (Tropix, Bedford, MA).

Two-dimensional Gel Electrophoresis—Cells were washed twice with PBS and pelleted by centrifugation. Cell pellets were resuspended in ReadyPrep reagent 3 from Bio-Rad containing 5 M urea, 2 M thiourea, 2% CHAPS, 2% SB 3–10, 40 mM Tris, and 0.2% Bio-Lyte 3/10 ampholyte. IPG strips (11 cm) with pH ranges 4 to 7 and a PROTEAN IEF Cell (Bio-Rad) were used for isoelectric focusing. Isoelectric focusing was performed using a two-phase protocol: (i) 250 V for 10 min, and (ii) 250-8000 V slow ramping voltage gradient to accumulate 35,000 total volt-hours. The focused IPG strips were equilibrated in reducing reagent (37.5 mM Tris-HCl, pH 8.8, 6 M urea, 2% SDS, 20% glycerol, 130 mM dithiothreitol) and alkylation reagent (37.5 mM Tris-HCl, pH 8.8, 6 M urea, 2% SDS, 20% glycerol, 135 mM iodoacetamide) before the second SDS-PAGE dimension.

Immunofluorescence and Confocal Microscopy—Cells were fixed in 4% paraformaldehyde for 30 min at room temperature and permeablized with 0.1% Triton X-100 in PBS for 5 min. For γ-tubulin staining, cells were fixed with methanol for 10 min at −20 °C. To block nonspecific binding, cells were incubated with 1% bovine serum albumin in PBS for 30 min. Antibodies against Mad1, Plk1, Mad2, HA, γ-tubulin, Bub1, BubR1, Cenp-E, or CREST were added to cells at dilutions of 1:200 to 1:2000 and incubated for 1 h at room temperature. Cells were washed three times with PBS and then probed with fluorescent (Alexa 488, Alexa 594, or Alexa 647)-conjugated secondary antibodies. Cell nuclei were stained with DAPI (Invitrogen). Cells on coverslips were mounted onto glass slides with ProLong Gold antifade reagents (Invitrogen), and slides were visualized using a Leica TCS-NP/SP confocal microscope.

Mass Spectrometry Analysis—Protein bands were excised and gel slices were washed successively with ultra-pure water and 100% acetonitrile, then reduced with 50 mM dithiothreitol and alkylated with 55 mM iodoacetamide. The material was dried in a SpeedVac, and rehydrated in a 12.5 ng/μl trypsin, 15 ng/μl elastase, or 5 ng/μl AspN/GluC solutions. Trypsin and AspN/GluC digests were carried out in 50 mM ammonium bicarbonate, 10% acetonitrile, pH 8.0. Elastase digests were performed under the same conditions without acetonitrile. Peptides were extracted 2 times with 25 μl of 50% acetonitrile, 5% formic acid and dried in a SpeedVac. Phosphopeptide enrichment was performed using the Phos-trap™ Phosphopeptide Enrichment kit (PerkinElmer Life Sciences) following the manufacturer's protocol. Phosphopeptides were resuspended in 20 μl of buffer A (5% acetonitrile, 0.1% formic acid, 0.005% heptafluorobutyric acid) and 3–6 μl were loaded onto a 12 cm × 0.075-mm fused silica capillary column packed with 5 μM diameter C-18 beads (The Nest Group, Southboro, MA). Peptides were eluted by applying a 0–80% linear gradient of buffer B (95% acetonitrile, 0.1% formic acid, 0.005% HFBA) at a flow rate of 150 μl/min

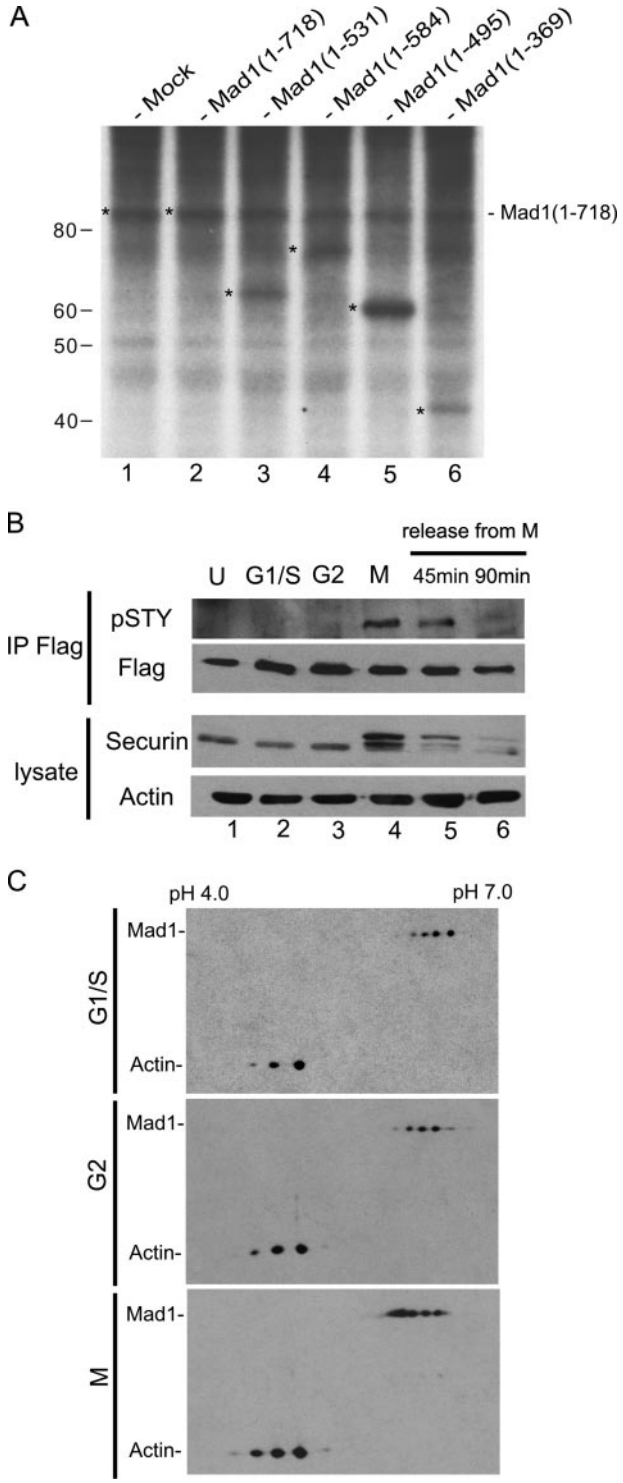

FIGURE 1. **Cell-cycle dependent phosphorylation of Mad1.** *A*, phosphorylation of human cell endogenous Mad1 (*lane 1*), and Mad1 in cells transfected with plasmid that express Mad1 wild type (WT, 1–718; *lane 2*) or the indicated Mad1 mutants (amino acids 1–531, 1–584, 1–495, and 1–369; *lanes 3–6*). Phosphorylated proteins were biosynthetically labeled with [^{32}P]orthophosphate. Mad1 WT and the indicated mutant proteins were immunoprecipitated using a mixture of two antibodies that recognize the N and C terminus of Mad1, respectively. The immunoprecipitates were analyzed by SDS-PAGE followed by autoradiography. ^{32}P-Incorporated bands of Mad1 WT and mutants are denoted by the *asterisk*. *B*, Mad1 was immunoprecipitated from a HeLa cell line stably expressing a FLAG-Mad1 transgene using anti-FLAG-agarose beads. The immunoprecipitates were electrophoresed and then immunoblotted using an αpSTY antibody that specifically recognizes a phosphorylated serine/threonine/or tyrosine residue. Immunoblotting using anti-FLAG (*Flag*) verified the immunoprecipitation of FLAG-Mad1. Cells were asynchronous (*U*), synchronized in G_1/S, G_2, M (nocodazole-arrested), or were released from nocodazole for 45 or 90 min, as indicated. Immunoblotting of securin was used to reflect cell cycle synchronization status, and blotting for actin was used to monitor equal sample loading. *C*, two-dimensional gel electrophoresis followed by immunoblotting of cell endogenous Mad1 from G_1/S, G_2, and M phase-enriched HeLa cells. Actin was used to align the positioning of the Mad1 two-dimensional spots. Compared with G_1/S- and G_2-synchronized cells, more Mad1 two-dimensional spots in M phase are shifted toward the cathode consistent with hyperphosphorylation and lowered isoelectric points (pI).

with a pre-column flow splitter resulting in a final flow rate of ~200 nl/min directly into the source. A LTQ^{TM} Linear Ion Trap (ThermoFinnigan, San Jose, CA) was run in an automated collection mode with an instrument method composed of a single segment and 5 data-dependent scan events with a full MS scan followed by 4 MS/MS scans of the highest intensity ions. Normalized collision energy was set at 35, activation Q was 0.250 with minimum full scan signal intensity at 1×10^5 with no minimum MS2 intensity specified. Dynamic exclusion was turned on utilizing a 3-min repeat count of 2 with the mass width set at 1.0 *m*/*z*. Sequence analysis was performed with TurboSEQUEST^{TM} (ThermoFinnigan, San Jose, CA) or MASCOT (Matrix Sciences, London, United Kingdom) using the non-redundant protein data base from the National Center for Biotechnology Information (NCBI) web site.

RESULTS

Cell Cycle-dependent Phosphorylation of Mad1—Mad1 was first reported to be phosphorylated upon SAC activation in *Saccharomyces cerevisiae* (6). To establish human Mad1 as a phosphoprotein, we employed classical [^{32}P]orthophosphate biosynthetic labeling of cultured cells followed by immunoprecipitation using a mixture of antibodies raised to the N and C terminus of Mad1 (αMad1-N and αMad1-C). HeLa cells were mock-transfected (Fig. 1*A*, *lane 1*), transfected with full-length Mad1 vector, or with vectors that express the indicated Mad1 deletion mutant (Fig. 1*A*, *lanes 2–6*). After biosynthetic labeling with [^{32}P]orthophosphate for 24 h, Mad1 protein was immunoprecipitated. Subsequent gel electrophoresis and autoradiography of the immunoprecipitates verified ^{32}P-incorporation into full-length Mad1 (both the cell endogenous and the transfected forms, Fig. 1*A*, *lanes 1–2*) and each of the transfected Mad1 deletion mutants (Fig. 1*A*, *lanes 3–6*). These results support the ambient phosphorylation of Mad1 in cultured cells.

To study the kinetics of Mad1 phosphorylation, we constructed a cell line (HeLa-FlagMad1) that stably expresses an integrated FlagMad1 vector. We enriched HeLa-FlagMad1 cells in various cell cycle phases, and immunoprecipitated Flag-Mad1 using monoclonal anti-FLAG-agarose beads. Mad1-phosphorylation was assessed first by Western blotting using an antibody (αpSTY) that recognizes a phosphorylated serine/threonine/or tyrosine residue. Indeed, the αpSTY antibody visualized a phosphorylated ~85-kDa Mad1 protein in M-cells, but did not detect phosphor-Mad1 in unsynchronized (U) cells or cells enriched in either G_1/S or G_2 (Fig. 1*B*, *lanes 1–3*). Interestingly, the level of phosphorylated Mad1 detected by αpSTY diminished progressively the longer HeLa-FlagMad1 cells were

released from nocodazole-induced mitotic arrest (Fig. 1*B*, *lanes 4–6*). These results suggest that αpSTY recognizes a phosphorylated Mad1 specific to the M-phase.

We next characterized Mad1 using two-dimensional isoelectric focusing gel electrophoresis (Fig. 1*C*). Mad1 proteins were "focused" to discrete isoelectric points and were visualized by Western blotting using αMad1-C serum. We compared the two-dimensional profiles of Mad1 in interphase (G_1/S and G_2) and M phase. In G_1/S and G_2 cells, Mad1 focused to 3 to 4 spots of varying intensities, consistent with multiple phosphorylation sites as suggested by the biosynthetic ^{32}P-incorporation data (Fig. 1*A*). In M-cells, the isoelectric points (pI) of Mad1 were shifted toward the cathode (pH 4.0, Fig. 1*C*), a finding consistent with hyperphosphorylation. Of note, the control focusing profiles of actin in the different samples were unchanged (Fig. 1*C*).

Mad1 Interacts with Plk1—Several mitotic kinases have been suggested to regulate the kinetochore localization of Mad1. These kinases include Bub1, BubR1, Mps1, and Plk1 (34–36). To gain insight into Mad1 phosphorylation, we asked whether Mad1 interacts with the various mitotic kinase(s).

We overexpressed Plk1, BubR1, Bub1, Aurora B, or Mps1 separately in cells with FLAG-tagged Mad1 and arrested the cells in M using nocodazole. Cell lysates were then immunoprecipitated for Mad1, and the co-precipitated proteins were analyzed. In these experiments, the Mad2 protein was employed as a positive control that co-immunoprecipitates with Mad1. Indeed, cell endogenous Mad2 was reproducibly seen with FLAG-Mad1 in all the assays (Fig. 2*A*, *lanes 2*, *4*, *6*, and *8*, and supplementary Fig. S1).

Our co-immunoprecipitations did reveal that Plk1, but not BubR1, Bub1, Aurora B, or Mps1, was associated with Mad1 (Fig. 2*A* and supplementary Fig. S1). Although a previous report had suggested that BubR1 phosphorylation in *Xenopus* egg extracts required Mad1 (37), we did not observe a Mad1-BubR1 co-immunoprecipitation (Fig. 2*A*, *lanes 5–8*). Similarly, whereas Bub1 has been reported to phosphorylate human Mad1 *in vitro* (38) and Mps1 has been shown to phosphorylate Mad1p in budding yeast (39), neither Bub1 nor Mps1 was co-immunoprecipitated with Mad1 from our M-arrested human cell lysates (Fig. S1). These findings support a preferential interaction between Mad1 and Plk1 that was not seen between Mad1 and the other mitotic kinases. However, our findings do not exclude the possibility that under other conditions Mad1 could interact with mitotic kinases other than Plk1.

To extend the results from the above overexpression experiments, we asked next whether cell endogenous Mad1 and Plk1 would similarly interact. An association between cell endogenous Mad1 and Plk1 in M phase was demonstrated by immunoprecipitating the former using a mixture of αMad1-N and αMad1-C antibodies (Fig. 2*B*). We observed that Plk1 co-precipitated with Mad1 from M phase-enriched cells (M) but not from asynchronous (U) cells (Fig. 2*B*). The results indicate a cell cycle-regulated Mad1-Plk1 interaction.

Mad1 is a coiled-coiled protein with a nuclear localization signal (amino acids 381–400) and two leucine zippers, positioned at 501–522 and 557–571, respectively (40) (Fig. 2*C*). To characterize the Plk1 interacting region of Mad1, we overex-

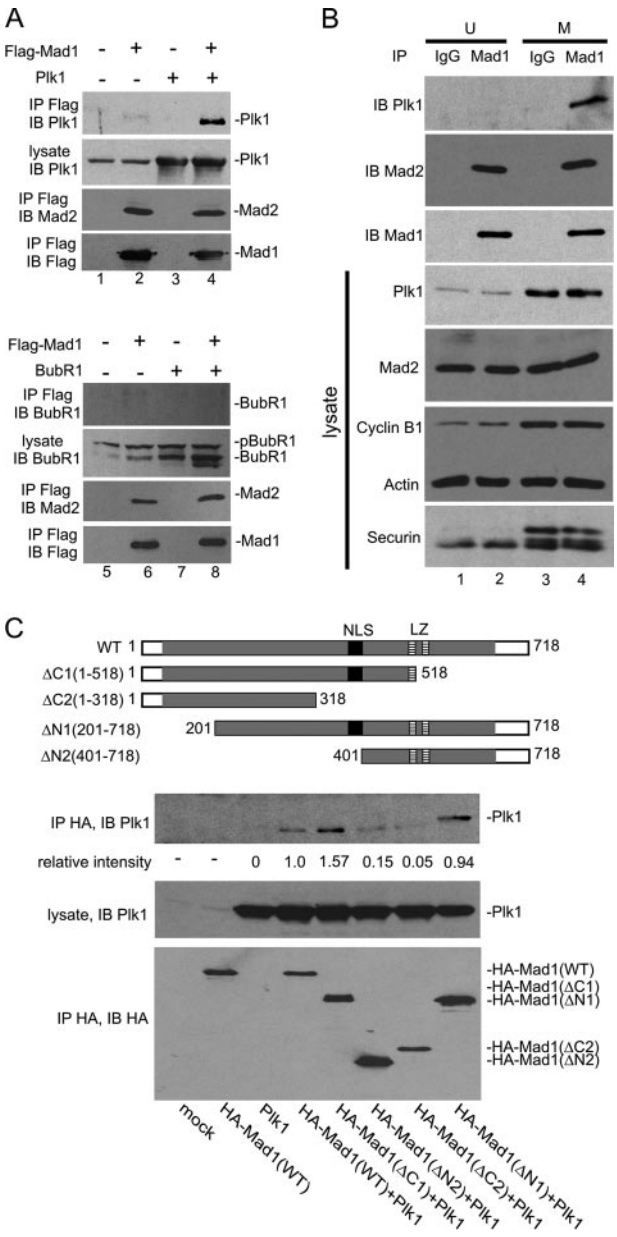

FIGURE 2. **Mad1 interacts with Plk1.** *A*, cells transfected with FLAG-Mad1 and/or Plk1 (untagged), or BubR1 (untagged) were enriched in M phase by nocodazole treatment. Immunoprecipitations (*IP*) were performed using anti-FLAG, and the immunoprecipitates were analyzed by Western blotting using anti-FLAG, anti-Mad2, anti-Plk1, or anti-BubR1 as indicated. Plk1 and Mad2 (*top panels*), but not BubR1 (*bottom panels*), were co-immunoprecipitated with Mad1. *B*, cell endogenous Mad1-Plk1 interaction was examined by co-immunoprecipitation using αMad1-N and αMad1-C antibodies. Nonspecific rabbit IgG was used as control. Cells were either asynchronous (*U*) or M-synchronized by nocodazole. Immunoblottings (*IB*) of transfected cell lysates were performed for Plk1, Mad2, cyclin B1, actin, and securin (*bottom 4 panels*). Immunoprecipitates of the same cell lysates were recovered using αMad1-N and αMad1-C antibodies, and these were immunoblotted for Plk1, Mad2, and Mad1 (*top 3 panels*) to show that Mad1-Plk1 interaction occurred preferentially in M. *C*, co-immunoprecipitation of Plk1 with Mad1 WT or the indicated Mad1 deletion mutants. Cells were mock transfected or transfected with the indicated expression plasmids (see labeling at bottom). HA-tagged WT and Mad1 deletion mutants (ΔN1:201–718, ΔN2:401–718, ΔC1:1–518, and ΔC2: 1–318; schematic illustration at *top*) were used. The immunoprecipitation/immunoblotting of the HA-tagged Mad1 proteins is shown in the *bottom panel*. The *middle panel* shows equal amounts of transfected Plk1 in each of the cell lysates. The *top panel* shows the amount of Plk1 recovered with the respective Mad1 immunoprecipitation. The relative intensities of the Plk1 band normalized to the immunoprecipitated HA-Mad1 signals are shown numerically *below* the *top gel panel*. Band intensities were quantified using ImageJ software.

pressed Plk1 separately with a HA-tagged WT Mad1 or one of several HA-tagged Mad1 deletion mutants (Fig. 2*C*, *top schematics*). We performed co-immunoprecipitations from cells transfected with these expression plasmids. The results revealed that a Mad1 deletion mutant removed in its carboxyl 400 amino acids (*i.e.* Mad1ΔC2, amino acids 1–318) failed to co-precipitate Plk1 (Fig. 2*C*), and that the Mad1ΔN2 mutant (containing amino acids 401–718) also captured Plk1 poorly. By contrast, two other Mad1 deletion mutants that retained the nuclear localization signal (*i.e.* ΔN1, ΔC1) co-precipitated Plk1 well (Fig. 2*C*). Whereas other interpretations are possible, these findings are consistent with a requirement of the central nuclear localization signal region of Mad1 for Plk1 interaction.

Plk1 Is Required for Mad1 Association with Spindle-unattached Kinetochores—Mad1 is found at nuclear pores in interphase cells and at spindle-unattached kinetochores in mitotic cells (13). To further characterize the Mad1-Plk1 interaction, we asked whether the two proteins co-localize inside cells. Prior to nuclear envelope breakdown, Plk1 was seen with Mad1 at the nuclear envelope (Fig. 3*A*, *panels 1–3*); later, as the cell entered prometaphase, both proteins were together at kinetochores (Fig. 3*A*, *panels 4–6*). Consistent with findings from others (13), Mad1, but not Plk1 (41), departed spindle-attached kinetochores as the cell moved into metaphase (Fig. 3*A*, *panels 7–9*). Interestingly, some Mad1 protein persisted with Plk1 at the spindle poles (Fig. 3*A*, *panels 1–9*, indicated by *arrows*; the centrosomes were verified by staining for γ-tubulin; Fig. 3*A*, *panels 10–18*). The functional significance of centrosomal Mad1-Plk1 co-localization remains to be investigated.

The Mad1 and Plk1 co-immunoprecipitations and co-localizations prompted us to ask if the latter could affect the function of the former. To investigate how Plk1 might influence Mad1 activity, we first used siRNA to knockdown Plk1. A >90% siRNA knockdown of Plk1 was achieved (Fig. 3*B*), and this depletion did not affect the level of cell endogenous Mad1 (Fig. 3*B*). Elsewhere, depletion of Plk1 has been reported to inhibit centrosome maturation and elicit prometaphase arrest with monoastral spindles (42). In our Plk1 knockdown cells, the mitotic index (cells staining positive for anti-phosphorylated histone H3 Ser^{10} (*red*, Fig. 3*C*)) increased from 6% in control siRNA cells to 30% in Plk1-siRNA cells (Fig. 3*C*). This increase agrees with previously described mitotic arrest observed when cells were Plk1-depleted (42). We noted a slight apparent accumulation of Mad1 in Plk1 knockdown cells. We do not know the reason for this small apparent increase, which may have resulted from some indirect changes in the cell arising as a consequence of Plk1 knock down.

We next examined the subcellular localization of Mad1 in Plk1 knockdown cells. Mad1 was found at spindle-unattached kinetochores in control siRNA cells (Fig. 3*D*, *panels 1–4*); however, in Plk1-siRNA cells, Mad1 was not concentrated at the kinetochores but was dispersed into the mitotic cytosol (Fig. 3*D*, *panels 5–8*). Similarly, the localizations of Mad2 mirrored those of Mad1 in both control RNAi (Fig. 3*D*, *panels 9–12*) and Plk1-RNAi (Fig. 3*D*, *panels 13–16*) cells. These Mad2 findings agree with a Plk1 requirement for Mad2-kinetochore localization as reported previously by some investigators (43, 44). By comparison, the cellular localizations of Bub1, BubR1, and Cenp-E were not changed in the Plk1-siRNA cells (supplementary Fig. S2 and Refs. 35, 43, and 44). Thus in our knockdown cells, Plk1 is selectively required for the kinetochore association of Mad1 and Mad2.

Plk1 has multiple functions including mitotic entry, spindle formation, and cytokinesis. These functions require the kinase activity of Plk1 (33, 41, 43, 45, 46). We asked next whether the kinase activity of Plk1 is also needed for the kinetochore association of Mad1. To address this question, we overexpressed a kinase-dead Plk1 mutant, K82M (33), and examined Mad1 localization in Plk1 K82M-transfected cells (Fig. 3*E*). Similar to Plk1 siRNA-transfected cells (Fig. 3*D*, *panels 5–8*), Plk1 K82M-expressing cells, when compared with control cells, phenocopied a >80% reduction in Mad1 staining at kinetochores (Fig. 3*E*, *panels 1–4*). One interpretation of these results is that overexpressed Plk1 K82M dominantly out competed the function of cell endogenous wild type (WT) Plk1. That a kinase-dead Plk1 mutant exerts a dominant phenotype supports the importance of the kinase activity of Plk1 for regulating the kinetochore localization of Mad1.

Mechanistically, it is possible that Plk1 influences Mad1 phosphorylation, thereby regulating its kinetochore function. To address the issue of phosphorylation more directly, we compared the two-dimensional gel profiles of Mad1 in Plk1-siRNA and control siRNA cells, enriched in prometaphase. As shown in Fig. 3*F*, the Mad1 "spots" in Plk1-siRNA cells, *versus* control siRNA cells, shifted with intensities toward the pH 7.0 isoelectric point (anode). This finding indicates reduced Mad1 phosphorylation with the knock down of Plk1.

Visualizing the Kinetochore Localization of Mad1 and Mad2 in the Presence of Plk1 Inhibitor GW843682X—The literature is controversial whether Plk1 depletion does (36, 43), or does not (42, 47) affect the kinetochore localization of Mad2. In our experiments above, both kinetochore staining of Mad2 and Mad1 are reduced in cells depleted for Plk1 (Fig. 3*D*). Indeed, the kinetochore presence in Mad2 was also lowered by overexpression of a kinase-dead Plk1 mutant (Fig. 3*E*). Because there is general agreement that Mad1 is needed to recruit Mad2 to kinetochores (14), our finding of a Plk1 requirement for the kinetochore association of Mad1 offers an explanation for why some investigators have reported that Plk1 reduction abrogated the Mad2 presence at kinetochores (36, 43, 45).

It is possible that the contrasting observations of Mad2 persistence at kinetochores upon Plk1 reduction (42, 47) could be due to variable efficiencies of Plk1 depletion in the different assays (as has been suggested by others (36, 44)). Intriguingly, two recent studies have reported that the association of Mad2 with kinetochores was unchanged when cells were treated with small molecule Plk1 inhibitors (48, 49), suggesting the dispensability of Plk1 for regulating this Mad2 activity. Due to MTA (material transfer agreement) disagreements between our institution (NIAID, National Institutes of Health) and the pharmaceutical firms that own those two inhibitors, we were denied their usage for our experiments. However, we could use an openly available ATP-competitive inhibitor of Plk1, GW843682X (50). GW843682X induces a transient G_2-M arrest (Ref. 50 and Fig. 4*A*) with mitotic spindle defects phenocopying, in part achieved with Plk1-siRNA (Fig. 3*C*). We, thus,

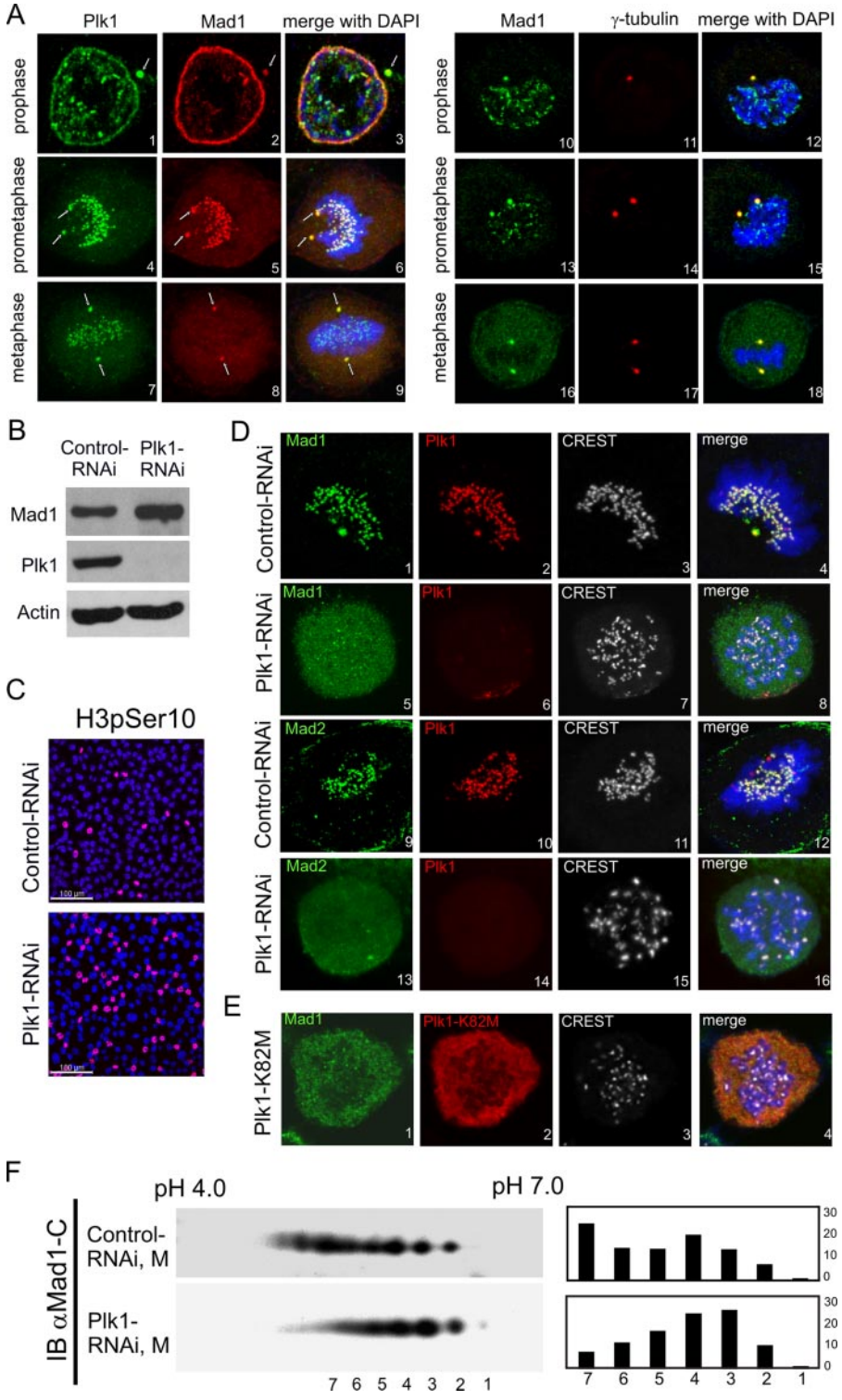

FIGURE 3. **Plk1 depletion reduced kinetochore localization of Mad1.** *A*, localizations of Mad1 and Plk1 in prophase, prometaphase, and metaphase are shown by immunofluorescent staining. DNA was stained with DAPI (*blue*). Plk1 co-localized with Mad1 at the nuclear envelope as the nuclear envelope commenced breakdown (prophase; *panels 1–3*). The two proteins co-stained at the kinetochores and spindle poles in prometaphase (*panels 4–6*), and at the spindle poles in metaphase (*panels 7–9*). During metaphase, Plk1, but not Mad1, remained at the kinetochores. Co-stainings of Mad1 and γ-tubulin at the spindle poles are shown in *panels 10–18*. The sum of *z*-stack images is shown. *B*, greater than 90% depletion of Plk1 by Plk1-siRNA was seen 24 h after siRNA transfection. *C*, Plk1 depletion induced mitotic arrest. Cells transfected with control or Plk1-siRNA were immunostained with anti-histone H3 phospho-Ser[10] antibody (*red*) to visualize cells in M. Approximately 30% of Plk1-siRNA cells in M were compared with 6% in control siRNA cells. DNA was stained with DAPI (*blue*). *D*, HeLa cells were transfected with control siRNA or Plk1-siRNA and then immunostained for Mad1/2 (*green*), Plk1 (*red*), and centromere marker CREST (*gray*). DNA was stained by DAPI (*blue*). Note the localization of Mad1 (*panel 1*) and Mad2 (*panel 9*) at kinetochores in control RNAi cells, and the dispersion of Mad1 (*panel 5*) and Mad2 (*panel 13*) from kinetochores in Plk1-RNAi cells. *E*, HeLa cells were transfected with a kinase-dead Plk1-K82M mutant and were immunostained for Mad1 (*green*), Plk1 (*red*), and centromere marker CREST (*gray*). DNA was stained by DAPI (*blue*). Sum of *z*-stack images is shown. *F*, two-dimensional gel electrophoreses of cell endogenous Mad1 in control RNAi (*Control-RNAi*, *M*) or Plk1-RNAi cells treated with nocodazole (*Plk1-RNAi*, *M*). Relative intensities (compared with total) of each two-dimensional spot (as numbered) were quantified using ImageJ software and are shown in the *bar graph* at *right*. *IB*, immunoblot.

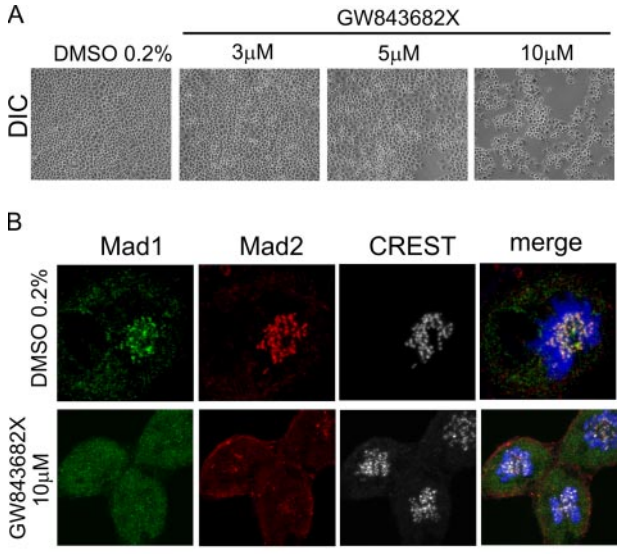

C

Conc. GW843682X	Mitotic Index	Mad1/Mad2 at kinetochores in M
0 μM	4%	100%
3 μM	12%	45%
5 μM	45%	18%
10 μM	92%	5%

FIGURE 4. **Plk1 inhibitor GW843682X reduced kinetochore association of Mad1 and Mad2.** *A*, light-field images of HeLa cells treated with Plk1 inhibitor GW843682X at various concentrations for 24 h. A dose-dependent increase in cell visually scored as being in mitosis was observed at higher concentrations of GW843682X. *B*, localization of Mad1 (*green*) and Mad2 (*red*) in the presence of GW843682X. CREST (*gray*) serum was used to visualize centromeres. DAPI is in *blue*. Sum of *z*-stack images is shown. A significant reduction in kinetochore association of Mad1 and Mad2 was observed with 10 μM GW843862X. *C*, an enumeration of the mitotic indices and the frequency of Mad1/2 staining at kinetochores in 0, 3, 5, and 10 μM GW843862X. For kinetochore staining 100 mitotic cells were analyzed in each of the treatment conditions. *DIC*, differential interference contrast.

examined Mad1/2 localization in GW843682X-treated cells. Indeed, cells were arrested in M phase by GW843682X in a dose-dependent manner (Fig. 4, *A* and *C*), and GW843682X-treated cells showed reduced kinetochore staining of Mad1 and Mad2 (Fig. 4*B*). A summary of the resulting mitotic indices and Mad1/2 kinetochore staining is presented in Fig. 4*C*. These GW843682X results are consistent with the findings from Plk1-siRNA and the Plk1 K82M mutant (Fig. 3), but they differ with the Plk1 inhibitor results from others (48, 49). Although we do not understand the reasons for the differences, they may be due partly to the different cell systems employed, or they may arise from inefficiencies of kinase inhibition and/or additional off-target specificities that can frequently occur with small molecule kinase inhibitors (51). Nevertheless, within our experimental system, the three independent ways to inhibit Plk1 function (siRNA, kinase-dead dominant negative mutant, and small molecule inhibitors) all produced similar reductions in Mad1 and Mad2 localization at kinetochores.

Identification of Phosphorylated Residues in Mad1—The collective results above do indicate that Mad1 phosphorylation and the kinase activity of Plk1 are important for SAC function of Mad1. We next wished to identify the phosphorylated residues in Mad1 and ask whether their phosphorylation is affected by Plk1. Toward these aims, we immunoprecipitated FLAG-tagged Mad1 from HeLa cells transfected without or with a Plk1 expression vector. The immunoprecipitated Mad1 was treated with protease, and the resulting phosphopeptides were analyzed by tandem mass spectrometry (MS/MS) (see "Experimental Procedures"). Using this approach, we completed a 90% coverage (650 of 718 amino acids) of Mad1. Within the sensitivity of this assay, the MS/MS results revealed Ser^{428}, Ser^{699}, and Thr^{708} as Mad1 phosphor-residues in mock-transfected cells, and Ser^{22}, Ser^{29}, Ser^{428}, Ser^{699}, Thr^{680}, and Thr^{708} as phosphorylated amino acids in Plk1-transfected cells. (The phosphopeptide sequences identified by MS/MS are listed in Fig. 5*A*; an illustrative MS/MS example spectrum that identified Thr^{680} phosphorylation is provided in supplementary Fig. S3A.) Thus Mad1 is phosphorylated at multiple residues, and its phosphor-profile is changed when Plk1 is overexpressed.

To ask if Mad1 could be a direct substrate for Plk1 *in vitro*, we immunoprecipitated overexpressed HA-tagged Mad1 from human cells and performed an *in vitro* kinase assay using commercially purchased purified bioactive Plk1. Compatible with the *in vivo* findings, the *in vitro* results are in part consistent with the ability of Plk1 to phosphorylate Mad1 directly (supplementary Fig. S3B).

Our MS/MS results agree with the previously reported Ser^{428} phosphorylation in Mad1 (52). However, in our experiments, phosphorylation of Ser^{428} was not influenced by Plk1 overexpression. Alignment of the sequences surrounding Ser^{22}, Ser^{29}, and Thr^{680} (the three amino acids whose phosphorylation appears to be influenced by Plk1) from different organisms (*Homo sapiens*, *Mus musculus*, *Xenopus laevis*, and *Drosophila melanogaster*; Fig. 5*B*) showed that Ser^{22} and Thr^{680} are well conserved, whereas Ser^{29} is less so. This suggests that phosphorylation at some of these residues may be maintained across different species.

To understand better the significance of Mad1 phosphorylation, we wondered if any of the six identified phosphor-residues in Mad1 might influence its kinetochore localization. To address this question, we reasoned that if phosphorylation at one or more of the six sites is needed for Mad1 attachment to kinetochores, then mutation of the responsible residue(s) to an amino acid incapable of being phosphorylated should create a Mad1 mutant(s) that cannot associate with spindle-unattached kinetochores. We, thus, individually mutated all 6 Mad1 phosphor-sites and tested the ability of each mutant to locate at kinetochores.

Because Mad1 can homodimerize (12, 30), to avoid complex interpretations that could emerge from a mutant Mad1 protein dimerizing with a cell endogenous WT Mad1 moiety, we treated cells first with Mad1-siRNA for 48 h prior to a second transfection with either a Mad1 WT or mutant expressing plasmid (Fig. 5*C*). Mad1 siRNA transfection showed a 70–75% knockdown of its target protein (Fig. 5*C*; however, the actual amount knocked down in the successfully transfected cells is probably closer to >90% because only 70% of the bulk cells were successfully transfected by siRNA; data not shown). We then immunostained cells transfected with siRNA for the transfected Mad1 proteins. In interphase cells, all six transfected Mad1 mutants decorated the nuclear periphery, in a manner indistinguishable from wild type Mad1 (supplementary Fig. S4).

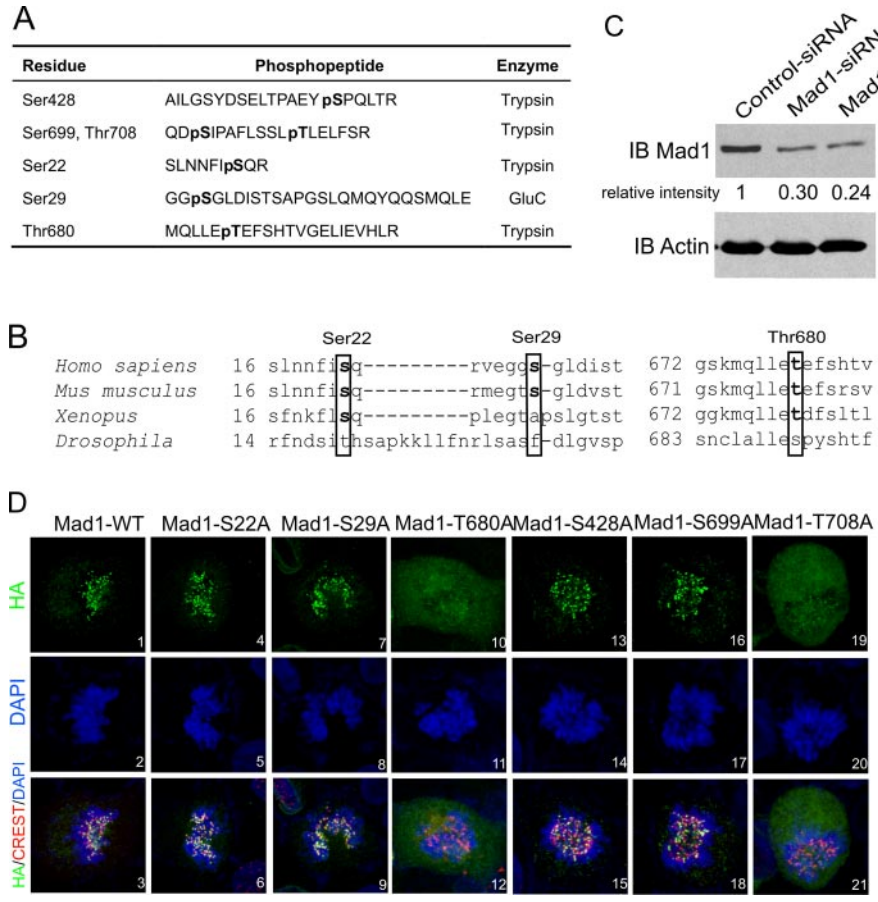

FIGURE 5. **Identification of phosphorylated residues in Mad1 by LC-MS/MS spectrometry.** *A*, phosphopeptides identified by MS/MS from FLAG-Mad1 immunoprecipitated (*IP*) from cells without or with Plk1 overexpression. Mad1 phosphorylation at Ser^{428}, Ser^{699}, and Thr^{708} was seen in mock transfected cells. Three additional phosphorylation sites, Ser^{22}, Ser^{29}, and Thr^{680} were identified in cells overexpressing transfected Plk1. The proteases used to generate the respective phosphopeptides are indicated. *B*, sequence alignment of Ser^{22}, Ser^{29}, Thr^{680} (in *boxes*) and their surrounding residues in Mad1 from *H. sapiens*, *M. musculus*, *X. laevis*, and *D. melanogaster*. *C*, depletion of cell endogenous Mad1 by siRNA. Two sets of Mad1 siRNA duplex were used (as described under "Experimental Procedures"). A ~70% knockdown in the bulk cell culture was achieved 48 h after transfection. *D*, subcellular distributions of HA-tagged (*green*) Mad1-WT or S22A, S29A, T680A, S428A, S699A, and T708A mutants in cells knocked down for endogenous Mad1 using siRNA. CREST serum was used to stain centromeres (*red*). DNA is in *blue*. Sum of *z*-stack images is shown. *IB*, immunoblot.

However, in mitotic cells, visibly reduced kinetochore staining was observed for the Mad1 T680A mutant (the great majority of T680A was dispersed into the mitotic cytosol; Fig. 5*D*, *panels 10–12*). On the other hand, the S22A, S29A, S428A, and S699A mutants, like WT Mad1, were seen at kinetochores (Fig. 5*D*). We also saw reduced kinetochore association by the T708A mutant (Fig. 5*D*, *panels 19–21*), suggesting that phosphorylation at this residue also influences the location at kinetochores for Mad1.

The Mad1 T680A Mutant Is Attenuated for SAC Function—SAC function requires Mad1 localization to kinetochores. Accordingly, a Mad1 mutant that cannot associate with kinetochores is expected to be checkpoint defective. To verify this expectation, we first knocked down cell endogenous Mad1 by siRNA, and then introduced, by a second transfection 48 h later WT Mad1 or mutant Mad1 transgenes into cells. The SAC activity of the cells was assayed by monitoring for nocodazole-induced mitotic arrest (Fig. 6, *A* and *B*). Cells with intact SAC would manifest efficient arrest, whereas cells with deficient SAC would not. By immunostaining for histone H3 phosphorylated on Ser^{10} as a marker, we identified cells that are in mitosis (Fig. 6*A*). Indeed, knockdown of Mad1 lowered the mitotic index of such cells, compared with control cells, treated with nocodazole (Fig. 6*A*, compare *panels 4–6* to *panels 1–3*; Ref. 53), consistent with a reduced SAC function. Informatively, overexpression of WT Mad1, Mad1-S22A, or Mad1-S29A, but not Mad1-T680A, in these Mad1 knockdown cells reconstituted SAC function as measured by an increase in nocadozole-induced mitotic index (Fig. 6, *A* and *B*). Thus the T680A mutation, unlike the S22A or S29A change, is inactivating the SAC function for Mad1. To ask further if phosphorylation of Thr^{680} contributes to SAC, we mutated threonine 680 to glutamate, thus creating an amino acid change that mimics phosphorylation. We next tested the Mad1-T680E mutant for function. Unlike the T680A mutant that reduced the cells' sensitivity to nocodazole-induced M-arrest, cells expressing the Mad1-T680E mutant showed the expected nocodazole-induced M-arrested phenotype (Fig. 6*A*, *panels 18–21*). This result is compatible with the interpretation that phosphorylation of Thr^{680} is important for the SAC activity of Mad1.

DISCUSSION

Mad1 is a SAC component whose role remains incompletely understood. Unlike other SAC proteins (*e.g.* Mps1, Bub1, and Cdc20), which are expressed selectively just prior to the onset of mitosis and then degraded rapidly during/after chromosome separation (54–57), human Mad1 is expressed continuously throughout the cell cycle, suggesting that its regulation cannot wholly be exerted via simple synthesis and degradation. A mechanism for Mad1 regulation may reside with changing its subcellular locations during the cell cycle. Accordingly, in interphase, Mad1 is at the nuclear pore complex, whereas in mitosis, Mad1 and its partner Mad2 protein move to spindle-unattached kinetochores. Currently, it is generally agreed that Mad1 is required to convey Mad2 to kinetochores (13, 14) and that the kinetochore localization of Mad2 is needed for the SAC function of the cell (17). What remains unclear are the requirements for the movement of Mad1 to kinetochores.

Some recent studies have begun to clarify the hierarchy of protein coalescence at kinetochores (58, 59). For example, in cell-free *Xenopus* extracts, Mps1 and Bub1 are loaded first on

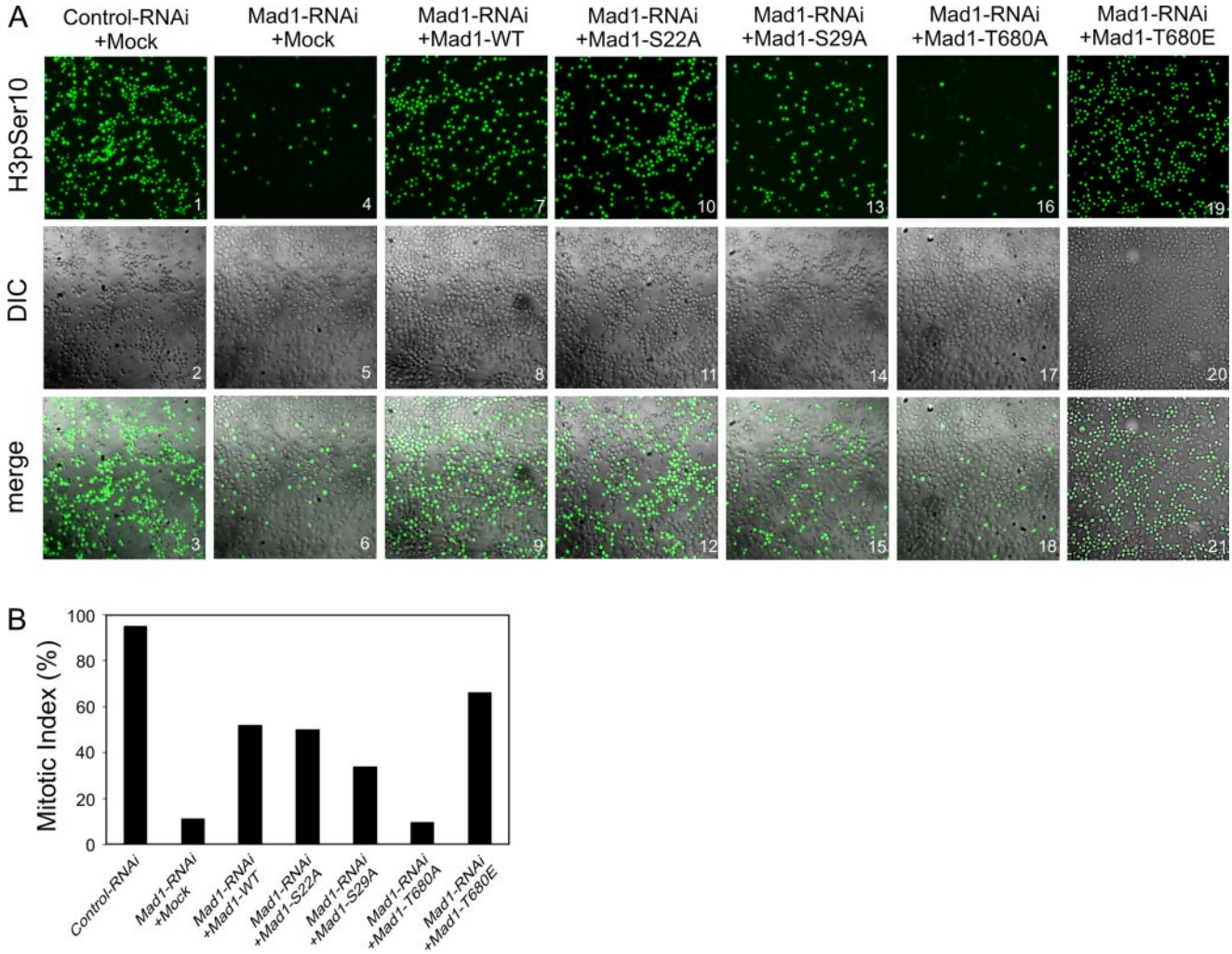

FIGURE 6. **Mutation of Mad1 Thr^{680} abrogated SAC activity.** *A*, mitotic indices of cells expressing Mad1-WT, Mad1-S22A, Mad1-S29A, Mad1-T680A, or Mad1-T680E after siRNA knockdown of cell endogenous Mad1 protein. Cells were pre-treated with Mad1-RNAi for 48 h and then transfected with Mad1-WT/mutants for another 24 h, followed by nocodazole (200 nM) treatment. 24 h later, cells were fixed and stained with anti-histone H3 phospho-Ser^{10} antibody (*green*) to visualize mitotic cells. Mitotic indices were scored (1000 cells were counted in each case) in *panel B*. *DIC*, differential interference contrast.

kinetochores followed by BubR1 and Plx1 (the *Xenopus* homologue of Plk1), and then finally Mad1 and Mad2 (36). Our current study adds further detail to the assembly events in human cells by suggesting that phosphorylation of Mad1 at threonine 680 and 708 may be important for the protein to engage kinetochores. In our investigation, we also found that Mad1 co-immunoprecipitated with Plk1, that knockdown of Plk1 in human cells abolished both Mad1 and Mad2 localization to kinetochores, and that phosphorylation of Mad1 at Thr^{680}, but not 708, was enhanced by Plk1 overexpression. These results suggest that Plk1 is influential of Mad1 phosphorylation. Nevertheless, we were puzzled that the amino acid motif surrounding Thr^{680} in Mad1 is inconsistent with a typical Plk1 target (60–62), raising the possibility that Plk1-enhanced Mad1 phosphorylation is either atypical or that the phosphorylation occurs indirectly via other kinases. We note that our two-dimensional gel results are consistent with Mad1 being phosphorylated at multiple amino acid residues. Currently, although our data support that the kinase activity of Plk1 is important, they do not exclude that other kinases also contribute to Mad1 phosphorylation and function. In this regard, we note that the kinase activity of Mps1 has been recently reported to be important for the kinetochore localization of Mad2, but not of Mad1 (63).

Plk1 function is important for normal mitotic progression. Indeed, cells arrest in mitosis when Plk1 is depleted by siRNA or when Plk1 function is interrupted or by kinase inhibitors (45) (Figs. 3*C* and 4*A*). However, it has been unclear what specific Plk1 downstream steps are responsible for the observed mitotic arrest and whether Mad2-APC/C interaction could account for this finding. Because congression of Mad1 and Mad2 to kinetochores is a pre-requisite for a Mad2-mediated mitotic arrest exerted via its inhibition of the proteasomal activity of p55CDC-APC/C (64, 65), our current results that a failure by either Mad1 or Mad2 to locate to kinetochores when Plk1 is depleted imply that the Mad1/2-APC/C (66) unlikely explains the mitotic arrest seen upon Plk1 depletion. Thus, a Plk1 depletion-triggered mitotic arrest probably does not emanate from the Mad2-microtubule-attachment sensing pathway, but might instead arise from the BubR1-microtubule-tension sensing pathway (66, 67). Compatible with this interpretation are two studies that reported that a Plk1-BubR1 interaction acted in

tension sensing and in the stabilization of kinetochore-microtubule engagement (43, 68).

Plk1 overexpression is a common finding in cancers (69). Aberrant expression of Mad1 (21, 22), Mad2 (70, 71), and the loss of SAC function (72, 73) are also seen in human tumors. Our data suggest that overexpressed Plk1 in tumors may further impact SAC function through an influence on Mad1 phosphorylation. Indeed, the investigation of Mad1 phosphorylation status and its effect on SAC function in primary human malignancies that overexpress Plk1 warrants future study.

Finally, our results when viewed with the previous finding on Mad2 (65) suggest that Mad1 and Mad2 activities may be controlled significantly through phosphorylation. However, phosphorylation appears to be inactivating for Mad2, but activating for Mad1. Phosphorylation of APC/C also appears to be important for its mitotic function (74). Indeed, additional informative insights likely will emerge from further examination of this post-translational mechanism in mitosis.

Acknowledgments—We thank Dr. Wei Dai, Department of Environmental Medicine, New York University School of Medicine, for providing the pcDNA-BubR1 plasmid, and members of the Jeang laboratory and Dr. Greg Reyes for readings of this manuscript.

REFERENCES

1. Chi, Y. H., and Jeang, K. T. (2007) *J. Cell. Biochem.* **102,** 531–538
2. Kops, G. J., Weaver, B. A., and Cleveland, D. W. (2005) *Nat. Rev. Cancer* **5,** 773–785
3. Yuen, K. W., Montpetit, B., and Hieter, P. (2005) *Curr. Opin. Cell Biol.* **17,** 576–582
4. Iwanaga, Y., Chi, Y. H., Miyazato, A., Sheleg, S., Haller, K., Peloponese, J. M., Jr., Li, Y., Ward, J. M., Benezra, R., and Jeang, K. T. (2007) *Cancer Res.* **67,** 160–166
5. Rudner, A. D., and Murray, A. W. (1996) *Curr. Opin. Cell Biol.* **8,** 773–780
6. Hardwick, K. G., and Murray, A. W. (1995) *J. Cell Biol.* **131,** 709–720
7. Sironi, L., Mapelli, M., Knapp, S., De Antoni, A., Jeang, K. T., and Musacchio, A. (2002) *EMBO J.* **21,** 2496–2506
8. Iouk, T., Kerscher, O., Scott, R. J., Basrai, M. A., and Wozniak, R. W. (2002) *J. Cell Biol.* **159,** 807–819
9. Hardwick, K. G., Li, R., Mistrot, C., Chen, R. H., Dann, P., Rudner, A., and Murray, A. W. (1999) *Genetics* **152,** 509–518
10. Li, Y., and Benezra, R. (1996) *Science* **274,** 246–248
11. Wang, Y., and Burke, D. J. (1995) *Mol. Cell. Biol.* **15,** 6838–6844
12. Sironi, L., Melixetian, M., Faretta, M., Prosperini, E., Helin, K., and Musacchio, A. (2001) *EMBO J.* **20,** 6371–6382
13. Campbell, M. S., Chan, G. K., and Yen, T. J. (2001) *J. Cell Sci.* **114,** 953–963
14. Chung, E., and Chen, R. H. (2002) *Mol. Biol. Cell* **13,** 1501–1511
15. Luo, X., Tang, Z., Xia, G., Wassmann, K., Matsumoto, T., Rizo, J., and Yu, H. (2004) *Nat. Struct. Mol. Biol.* **11,** 338–345
16. Mapelli, M., Massimiliano, L., Santaguida, S., and Musacchio, A. (2007) *Cell* **131,** 730–743
17. Yu, H. (2006) *J. Cell Biol.* **173,** 153–157
18. Peters, J. M. (2006) *Nat. Rev. Mol. Cell. Biol.* **7,** 644–656
19. King, R. W., Peters, J. M., Tugendreich, S., Rolfe, M., Hieter, P., and Kirschner, M. W. (1995) *Cell* **81,** 279–288
20. Osaka, F., Seino, H., Seno, T., and Yamao, F. (1997) *Mol. Cell. Biol.* **17,** 3388–3397
21. Coe, B. P., Lee, E. H., Chi, B., Girard, L., Minna, J. D., Gazdar, A. F., Lam, S., MacAulay, C., and Lam, W. L. (2006) *Genes Chromosomes Cancer* **45,** 11–19
22. Osaki, M., Inoue, T., Yamaguchi, S., Inaba, A., Tokuyasu, N., Jeang, K. T., Oshimura, M., and Ito, H. (2007) *Virchows Arch.* **451,** 771–779
23. Haller, K., Kibler, K. V., Kasai, T., Chi, Y. H., Peloponese, J. M., Yedavalli, V. S., and Jeang, K. T. (2006) *Oncogene* **25,** 2137–2147
24. Rangarajan, A., and Weinberg, R. A. (2003) *Nat. Rev. Cancer* **3,** 952–959
25. Rangarajan, A., Hong, S. J., Gifford, A., and Weinberg, R. A. (2004) *Cancer Cell* **6,** 171–183
26. Gaillard, S., Fahrbach, K. M., Parkati, R., and Rundell, K. (2001) *J. Virol.* **75,** 9799–9807
27. Leao, M., Anderton, E., Wade, M., Meekings, K., and Allday, M. J. (2007) *J. Virol.* **81,** 248–260
28. Marriott, S. J., and Semmes, O. J. (2005) *Oncogene* **24,** 5986–5995
29. Scarano, F. J., Laffin, J. A., Lehman, J. M., and Friedrich, T. D. (1994) *J. Virol.* **68,** 2355–2361
30. Jin, D. Y., Spencer, F., and Jeang, K. T. (1998) *Cell* **93,** 81–91
31. Kasai, T., Iwanaga, Y., Iha, H., and Jeang, K. T. (2002) *J. Biol. Chem.* **277,** 5187–5193
32. Matsuoka, M., and Jeang, K. T. (2007) *Nat. Rev. Cancer* **7,** 270–280
33. Seong, Y. S., Kamijo, K., Lee, J. S., Fernandez, E., Kuriyama, R., Miki, T., and Lee, K. S. (2002) *J. Biol. Chem.* **277,** 32282–32293
34. Palframan, W. J., Meehl, J. B., Jaspersen, S. L., Winey, M., and Murray, A. W. (2006) *Science* **313,** 680–684
35. Vigneron, S., Prieto, S., Bernis, C., Labbe, J. C., Castro, A., and Lorca, T. (2004) *Mol. Biol. Cell* **15,** 4584–4596
36. Wong, O. K., and Fang, G. (2006) *Mol. Biol. Cell* **17,** 4390–4399
37. Chen, R. H. (2002) *J. Cell Biol.* **158,** 487–496
38. Seeley, T. W., Wang, L., and Zhen, J. Y. (1999) *Biochem. Biophys. Res. Commun.* **257,** 589–595
39. Hardwick, K. G., Weiss, E., Luca, F. C., Winey, M., and Murray, A. W. (1996) *Science* **273,** 953–956
40. Iwanaga, Y., Kasai, T., Kibler, K., and Jeang, K. T. (2002) *J. Biol. Chem.* **277,** 31005–31013
41. van Vugt, M. A., and Medema, R. H. (2005) *Oncogene* **24,** 2844–2859
42. Sumara, I., Gimenez-Abian, J. F., Gerlich, D., Hirota, T., Kraft, C., de la Torre, C., Ellenberg, J., and Peters, J. M. (2004) *Curr. Biol.* **14,** 1712–1722
43. Ahonen, L. J., Kallio, M. J., Daum, J. R., Bolton, M., Manke, I. A., Yaffe, M. B., Stukenberg, P. T., and Gorbsky, G. J. (2005) *Curr. Biol.* **15,** 1078–1089
44. Wong, O. K., and Fang, G. (2005) *J. Cell Biol.* **170,** 709–719
45. Eckerdt, F., and Strebhardt, K. (2006) *Cancer Res.* **66,** 6895–6898
46. Dai, W., Huang, X., and Ruan, Q. (2003) *Front. Biosci.* **8,** d1128–d1133
47. van Vugt, M. A., van de Weerdt, B. C., Vader, G., Janssen, H., Calafat, J., Klompmaker, R., Wolthuis, R. M., and Medema, R. H. (2004) *J. Biol. Chem.* **279,** 36841–36854
48. Lenart, P., Petronczki, M., Steegmaier, M., Di Fiore, B., Lipp, J. J., Hoffmann, M., Rettig, W. J., Kraut, N., and Peters, J. M. (2007) *Curr. Biol.* **17,** 304–315
49. Santamaria, A., Neef, R., Eberspacher, U., Eis, K., Husemann, M., Mumberg, D., Prechtl, S., Schulze, V., Siemeister, G., Wortmann, L., Barr, F. A., and Nigg, E. A. (2007) *Mol. Biol. Cell* **18,** 4024–4036
50. Lansing, T. J., McConnell, R. T., Duckett, D. R., Spehar, G. M., Knick, V. B., Hassler, D. F., Noro, N., Furuta, M., Emmitte, K. A., Gilmer, T. M., Mook, R. A., Jr., and Cheung, M. (2007) *Mol. Cancer Ther.* **6,** 450–459
51. Bain, J., Plater, L., Elliott, M., Shpiro, N., Hastie, C. J., McLauchlan, H., Klevernic, I., Arthur, J. S., Alessi, D. R., and Cohen, P. (2007) *Biochem. J.* **408,** 297–315
52. Nousiainen, M., Sillje, H. H., Sauer, G., Nigg, E. A., and Korner, R. (2006) *Proc. Natl. Acad. Sci. U. S. A.* **103,** 5391–5396
53. Kienitz, A., Vogel, C., Morales, I., Muller, R., and Bastians, H. (2005) *Oncogene* **24,** 4301–4310
54. Weinstein, J. (1997) *J. Biol. Chem.* **272,** 28501–28511
55. Wu, H., Lan, Z., Li, W., Wu, S., Weinstein, J., Sakamoto, K. M., and Dai, W. (2000) *Oncogene* **19,** 4557–4562
56. Stucke, V. M., Sillje, H. H., Arnaud, L., and Nigg, E. A. (2002) *EMBO J.* **21,** 1723–1732
57. Tang, Z., Shu, H., Oncel, D., Chen, S., and Yu, H. (2004) *Mol. Cell* **16,** 387–397
58. Musacchio, A., and Salmon, E. D. (2007) *Nat. Rev. Mol. Cell. Biol.* **8,** 379–393
59. Chan, G. K., Liu, S. T., and Yen, T. J. (2005) *Trends Cell Biol.* **15,** 589–598
60. Elia, A. E., Rellos, P., Haire, L. F., Chao, J. W., Ivins, F. J., Hoepker, K., Mohammad, D., Cantley, L. C., Smerdon, S. J., and Yaffe, M. B. (2003) *Cell*

115, 83–95
61. Lowery, D. M., Mohammad, D. H., Elia, A. E., and Yaffe, M. B. (2004) *Cell Cycle* **3,** 128–131
62. Nakajima, H., Toyoshima-Morimoto, F., Taniguchi, E., and Nishida, E. (2003) *J. Biol. Chem.* **278,** 25277–25280
63. Tighe, A., Staples, O., and Taylor, S. (2008) *J. Cell Biol.,* **181,** 893–901
64. Kallio, M., Weinstein, J., Daum, J. R., Burke, D. J., and Gorbsky, G. J. (1998) *J. Cell Biol.* **141,** 1393–1406
65. Wassmann, K., and Benezra, R. (1998) *Proc. Natl. Acad. Sci. U. S. A.* **95,** 11193–11198
66. Skoufias, D. A., Andreassen, P. R., Lacroix, F. B., Wilson, L., and Margolis, R. L. (2001) *Proc. Natl. Acad. Sci. U. S. A.* **98,** 4492–4497
67. Fang, G. (2002) *Mol. Biol. Cell* **13,** 755–766
68. Elowe, S., Hummer, S., Uldschmid, A., Li, X., and Nigg, E. A. (2007) *Genes Dev.* **21,** 2205–2219
69. Strebhardt, K., and Ullrich, A. (2006) *Nat. Rev. Cancer* **6,** 321–330
70. Gemma, A., Hosoya, Y., Seike, M., Uematsu, K., Kurimoto, F., Hibino, S., Yoshimura, A., Shibuya, M., Kudoh, S., and Emi, M. (2001) *Lung Cancer* **32,** 289–295
71. Takahashi, T., Haruki, N., Nomoto, S., Masuda, A., Saji, S., Osada, H., and Takahashi, T. (1999) *Oncogene* **18,** 4295–4300
72. Cahill, D. P., Lengauer, C., Yu, J., Riggins, G. J., Willson, J. K., Markowitz, S. D., Kinzler, K. W., and Vogelstein, B. (1998) *Nature* **392,** 300–303
73. Weaver, B. A., and Cleveland, D. W. (2006) *Curr. Opin. Cell Biol.* **18,** 658–667
74. Steen, J. A., Steen, H., Georgi, A., Parker, K., Springer, M., Kirchner, M., Hamprecht, F., and Kirschner, M. W. (2008) *Proc. Natl. Acad. Sci. U. S. A.* **105,** 6069–6074